Radiology

ORIGINAL RESEARCH • GASTROINTESTINAL IMAGING

Deep Learning CT-based Quantitative Visualization Tool for Liver Volume Estimation: Defining Normal and Hepatomegaly

Alberto A. Perez, MD • Victoria Noe-Kim, BS • Meghan G. Lubner, MD • Peter M. Graffy, BS • John W. Garrett, PhD • Daniel C. Elton, PhD • Ronald M. Summers, MD, PhD • Perry J. Pickhardt, MD

From the Department of Radiology, University of Wisconsin School of Medicine & Public Health, E3/311 Clinical Science Center, 600 Highland Ave, Madison, WI 53792-3252 (A.A.P., V.N.K., M.G.L., P.M.G., J.W.G., P.J.P.); and Imaging Biomarkers and Computer-Aided Diagnosis Laboratory, Radiology and Imaging Sciences, National Institutes of Health Clinical Center, Bethesda, Md (D.C.E., R.M.S.). Received February 26, 2021; revision requested May 27; revision received August 4; accepted August 11. **Address correspondence to** P.J.P. (e-mail: *ppickhardt2@uwhealth.org*).

Supported in part by the Intramural Research Program of the National Institutes of Health (NIH) Clinical Center; used the high-performance computing capabilities of the NIH Biowulf cluster.

Conflicts of interest are listed at the end of this article.

See also the editorial by Sosna in this issue.

Radiology 2021; 000:1–7 • https://doi.org/10.1148/radiol.2021210531 • Content codes: GI CT

Background: Imaging assessment for hepatomegaly is not well defined and currently uses suboptimal, unidimensional measures. Liver volume provides a more direct measure for organ enlargement.

Purpose: To determine organ volume and to establish thresholds for hepatomegaly with use of a validated deep learning artificial intelligence tool that automatically segments the liver.

Materials and Methods: In this retrospective study, liver volumes were successfully derived with use of a deep learning tool for asymptomatic outpatient adults who underwent multidetector CT for colorectal cancer screening (unenhanced) or renal donor evaluation (contrast-enhanced) at a single medical center between April 2004 and December 2016. The performance of the craniocaudal and maximal three-dimensional (3D) linear measures was assessed. The manual liver volume results were compared with the automated results in a subset of renal donors in which the entire liver was included at both precontrast and postcontrast CT. Unenhanced liver volumes were standardized to a postcontrast equivalent, reflecting a correction of 3.6%. Linear regression analysis was performed to assess the major patient-specific determinant or determinants of liver volume among age, sex, height, weight, and body surface area.

Results: A total of 3065 patients (mean age ± standard deviation, 54 years ± 12; 1639 women) underwent multidetector CT for colorectal screening (n = 1960) or renal donor evaluation (n = 1105). The mean standardized automated liver volume ± standard deviation was 1533 mL ± 375 and demonstrated a normal distribution. Patient weight was the major determinant of liver volume and demonstrated a linear relationship. From this result, a linear weight-based upper limit of normal hepatomegaly threshold volume was derived: hepatomegaly (mL) = 14.0 × (weight [kg]) + 979. A craniocaudal threshold of 19 cm was 71% sensitive (49 of 69 patients) and 86% specific (887 of 1030 patients) for hepatomegaly, and a maximal 3D linear threshold of 24 cm was 78% sensitive (54 of 69) and 66% specific (678 of 1030). In the subset of 189 patients, the median difference in hepatic volume between the deep learning tool and the semiautomated or manual method was 2.3% (38 mL).

Conclusion: A simple weight-based threshold for hepatomegaly derived by using a fully automated CT-based liver volume segmentation based on deep learning provided an objective and more accurate assessment of liver size than linear measures.

Online supplemental material is available for this article.

Hepatomegaly is defined as abnormal enlargement of the liver that can result from a wide variety of inflammatory, infiltrative, neoplastic, and other conditions. Detecting a correlation between hepatomegaly and clinical and laboratory findings as well as between acute and subacute or chronic clinical course is essential. Imaging diagnosis of hepatomegaly is generally based on subjective assessment using cross-sectional modalities such as US or CT supplemented by various linear craniocaudal (CC) measurements. However, unidimensional (linear) assessment is a suboptimal method that does not completely reflect the complex morphology of this three-dimensional (3D) organ. As such, CC measurements may overestimate the size of the liver, as with the normal variant of a Riedel lobe configuration, or underestimate its size, as in the case of relative left lobe and caudate hypertrophy. Ultimately, it is reasonable that the best determinant of liver size is the liver volume. Previously, estimating the liver volume on the basis of cross-sectional imaging was a labor-intensive process. With use of deep learning algorithms, liver segmentation and volume assessment can now be accomplished in a fully automated manner, potentially rendering this approach both more efficient and likely more accurate than manual linear assessment.

Previous CT studies aimed to establish thresholds for normal liver volume in healthy adults but generally included small cohort sizes and/or used approaches that are manual or only partially automated (1–12). Other studies attempted to measure liver volume using fully automated CT-based techniques (13–15), with varying success.

Abbreviations

3D = three-dimensional, BSA = body surface area, CC = craniocaudal, CTC = CT colonography

Summary

Fully automated CT-based liver volume segmentation based on deep learning methods provided an objective and more accurate assessment of liver size than linear measures.

Key Results

- In a retrospective analysis of 3065 patients who underwent multidetector CT for colorectal screening (n = 1960, unenhanced) or renal donor evaluation (n = 1105, contrast-enhanced), patient weight was the major determinant of liver volume, allowing a weight-based upper limit of normal threshold for hepatomegaly: mL = 14.0 × (weight [kg]) + 979.
- Liver volumes measured using automated deep learning and manual methods were in close agreement, with a median difference of less than 3%.
- Linear estimates of liver size were inaccurate for determining the amount of liver tissue, as shown by the automated liver volume.

However, the purpose of these studies was to compare automated measurements with manual measurements, rather than characterize the liver size in large healthy populations.

The main purpose of our study was to establish the normal distribution of liver volumes in healthy adults using a fully automated CT-based artificial intelligence quantitative visualization tool and to suggest potential thresholds for hepatomegaly, considering patient-specific factors. We also assessed the performance of linear CT measurements for identifying cases of hepatomegaly according to these volume thresholds.

Materials and Methods

Study Patients

This investigation complied with the rules of the Health Insurance Portability and Accountability Act and was approved by the institutional review board at the University of Wisconsin and the Office of Human Subjects Research Protection at UW Health. The requirement for signed informed consent was waived for this retrospective assessment. The initial study cohort comprised consecutive generally healthy asymptomatic adult outpatients undergoing either unenhanced abdominal CT for colorectal cancer screening (CT colonography [CTC]) or postcontrast abdominal CT for potential renal (kidney) donation at a single medical center between April 2004 and December 2016. Patients who did not have the entire liver scanned at CT were excluded. Patients with missing data were excluded. Only one CT study was included per patient.

Basic demographic and clinical information (age, sex, weight, and height) was collected from the electronic health record. Body surface area (BSA) was calculated using the Mosteller method (16):

$$BSA\left(m^2\right) = \sqrt{\left(height\left[cm\right] \times weight\left[kg\right] / 3600\right)}.$$

CT Protocol

All CT studies were performed with eight- to 64-section multidetector–row scanners (GE Healthcare). The CT acquisition technique used has been previously described in detail (17,18). Briefly, for the study patients undergoing CTC, we used unenhanced supine CT performed with 120 kVp and modulated tube current (typically between 30 mA and 300 mA) to achieve a noise index of 50. For the renal donor group, we used the postcontrast parenchymal phase abdominal CT series, typically consisting of 120 kVp and modulated tube current (between 30 mA and 300 mA), with a noise index of 17–28, both based on patient size. The intravenous contrast agent was iohexol (Omnipaque, GE Healthcare). We also obtained a precontrast series for the renal donor protocol but typically did not include the entire liver. However, a subset of renal donor cases for which whole-liver pre- and postcontrast series were available was used to derive the small correction to convert unenhanced CTC liver volumes to a postcontrast equivalent (see following section). Before automated liver segmentation, we retrospectively reformatted all CT series to 3-mm-thick sections at 3-mm intervals.

Automated Liver Segmentation and Volume Assessment

The detailed description of the automated deep learning segmentation method for organ segmentation can be found elsewhere and includes a modified 3D U-Net and CycleGAN (19–21). The relevant code has been posted to *https://github.com/rsummers11/CADLab/tree/master/CT%20Liver%20Segmentation%20Software*. The deep learning algorithms used in this study have been previously developed, trained, and tested at the National Institutes of Health. No additional training, validation, or machine learning was required for this study, which precludes the need to repeat separate training and testing. This deep learning tool differs from an older tool that used traditional, manually designed image processing methods (5).

To enable processing of large 3D volumes with limited graphics processing unit memory, an initial strided convolution (step size 2) and a complementing final transposed convolution were added. Training data were obtained from the Medical Segmentation Decathlon project (22). Data augmentation was performed using 3D rotation, crop, elastic deformation, CycleGAN noncontrast image, and random flips. Model training and inference were performed on the National Institutes of Health Biowulf System high-performance computing cluster using four central processing unit threads and up to 48 graphics processing unit nodes (NVIDIA K80 or P100; graphics processing unit memory, 12 or 16 GB, respectively). The batch size was four, resolution was 256 × 256 × 192, and initial filters were 32. The initial learning rate was 0.0001, and training was performed for 10 000 iterations. All voxels designated as liver by the segmentation algorithm were analyzed, and the liver volume was computed. A mean Dice score of 0.887 ± 0.006 (standard deviation) was found in a prior validation report (21). To ensure the liver was completely included within the scanned range, at least one section without segmented liver was included, both superior and inferior to the segmented liver. To allow for quality assurance in individual scans, the tool provides a mask series that can be fused with the original imaging

series for visual inspection of the segmented liver section by section (Figs 1, 2). In general, intrahepatic vessels and focal hepatic lesions are included in the automated liver segmentation, which allows for similar handling regardless of whether intravenous contrast material was administered.

Additionally, the linear distance between the most cephalad and caudal sections containing segmented liver were used to automatically derive the true CC liver length. This automated true CC measurement is theoretically a better representation of liver size than typical CC values derived in practice, which represent the longest linear measurement contained on a single coronal section and may be angled in some. The automated tool also derives the longest linear dimension of the liver in 3D space (maximal 3D length in any plane), which would be difficult to obtain manually in practice.

Although this deep learning tool has been previously trained and tested, we sought further parallel validation by comparing the results with those of another validated semiautomated CT software tool (CT Liver Analysis, Philips IntelliSpace Portal) that requires manual correction by the user before final liver segmentation and volume determination (11,23). After initial automated segmentation of the entire liver by the software, the margins are then verified and easily manipulated if needed by using adjustable digital brush and eraser tools to add or subtract tissue volume, respectively. We compared the volume between this semiautomated software tool and the fully automated deep learning tool in a subset of postcontrast CT studies from the renal donor group.

Statistical Analysis

Summary statistics for demographic and clinical data were compiled. Stepwise multiple linear regressions were used to assess the relationships between demographic and clinical data and liver

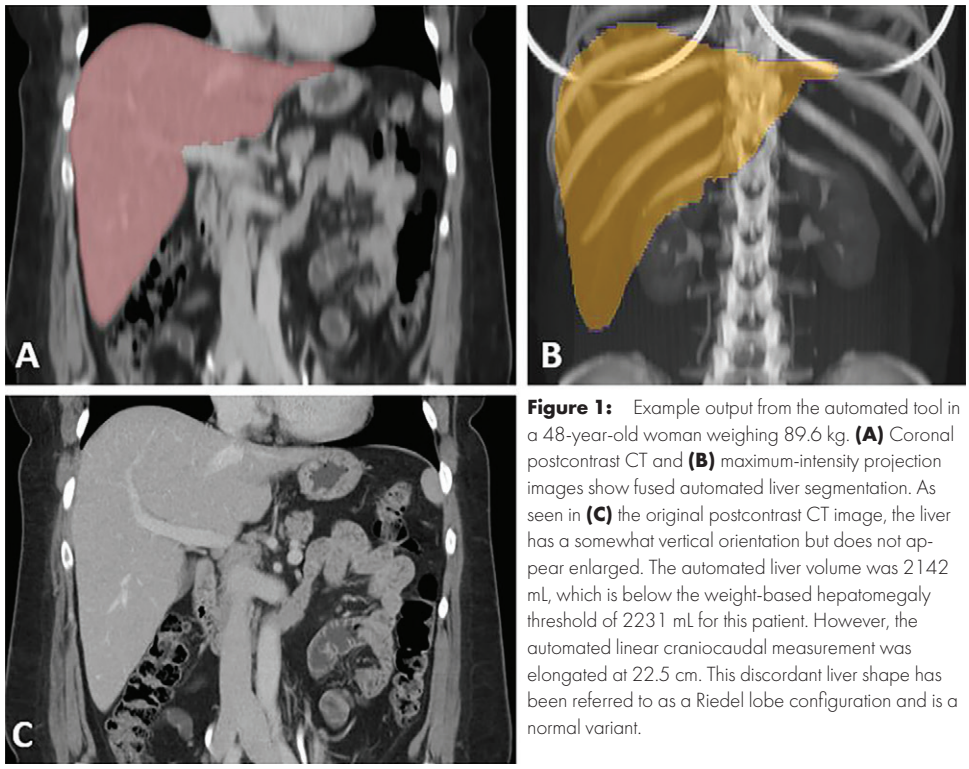

Figure 1: Example output from the automated tool in a 48-year-old woman weighing 89.6 kg. **(A)** Coronal postcontrast CT and **(B)** maximum-intensity projection images show fused automated liver segmentation. As seen in **(C)** the original postcontrast CT image, the liver has a somewhat vertical orientation but does not appear enlarged. The automated liver volume was 2142 mL, which is below the weight-based hepatomegaly threshold of 2231 mL for this patient. However, the automated linear craniocaudal measurement was elongated at 22.5 cm. This discordant liver shape has been referred to as a Riedel lobe configuration and is a normal variant.

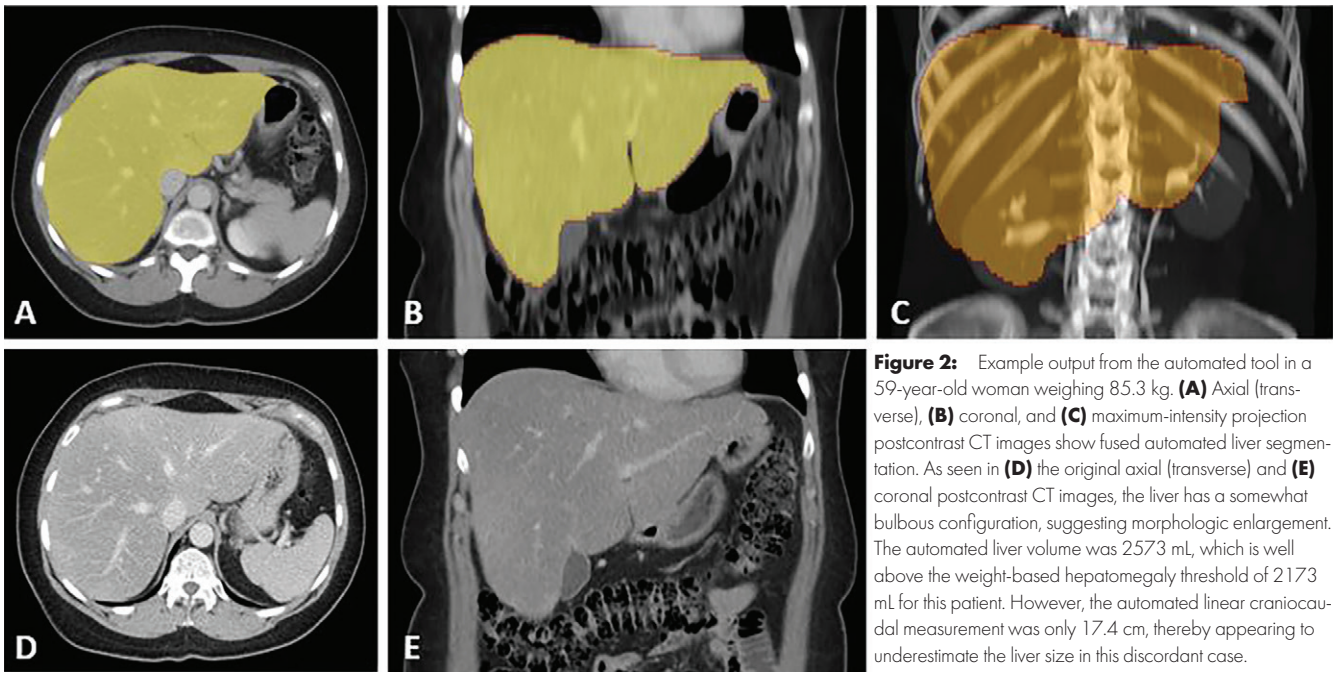

Figure 2: Example output from the automated tool in a 59-year-old woman weighing 85.3 kg. **(A)** Axial (transverse), **(B)** coronal, and **(C)** maximum-intensity projection postcontrast CT images show fused automated liver segmentation. As seen in **(D)** the original axial (transverse) and **(E)** coronal postcontrast CT images, the liver has a somewhat bulbous configuration, suggesting morphologic enlargement. The automated liver volume was 2573 mL, which is well above the weight-based hepatomegaly threshold of 2173 mL for this patient. However, the automated linear craniocaudal measurement was only 17.4 cm, thereby appearing to underestimate the liver size in this discordant case.

Table 1: Patient Demographics

Parameter	Value
Sex*	
Male	1426
Female	1639
Age (y)	
Mean ± standard deviation	54 ± 12
Median and interquartile range	55 (50–62)
Range	18–95
Weight (kg)	79.4 ± 17.7
Height (m)	1.71 ± 0.10
Body surface area (m^2)	1.9 ± 0.3

Note.—The study included 3065 patients. Unless otherwise specified, data are means ± standard deviations.
* Data are numbers of patients.

volumetric data. Simple least-squares linear regression was performed to show the mean trend between the dominant predictive clinical factor or factors from the initial multiple regressions and liver volume. Given these results, an upper limit of normal line was created, defined by adding two times the standard deviation of the residuals of the constant (y-intercept) to the final linear regression. Outliers with liver volumes above the upper limit of normal line were classified as having hepatomegaly for the remainder of the analysis. Contingency tables were constructed to assess the performance of the automatically acquired CC and maximal 3D linear measurements as predictors of hepatomegaly against the volumetric definition provided earlier. All statistics were calculated on IBM SPSS Statistics 26 software. $P < .05$ was used for determining statistically significant difference.

To evaluate intrapatient changes in liver volume after intravenous contrast material administration, we used a subset of renal donor scans in which the entire liver was included on both precontrast and postcontrast series. We performed linear least-squares regression analysis to compare pre- and postcontrast volume results (Appendix E1 [online]). This minor correction (3.6%) was then applied to the scans from the group that underwent unenhanced CTC, resulting in postcontrast-equivalent volumes that allowed the two subsets to be combined for all subsequent analyses.

Results

Patient Characteristics

Among the 10 473 total asymptomatic adult outpatients undergoing either unenhanced abdominal CT for colorectal cancer screening (n = 9223) or postcontrast abdominal CT for potential renal donation (n = 1250), 7406 patients were excluded for CT scans that did not contain the entire liver (n = 7261 from CTC group and n = 145 from renal donor group), and two patients from the CTC group were excluded due to missing demographic or clinical information (Fig E1 [online]). The final sample consisted of 3065 asymptomatic adults (mean age ± standard deviation, 54 years ± 12; 1426 men, 1639 women). The average patient height ± standard deviation was 1.71 m ± 0.10, and the average patient weight was 79.4 kg ± 17.7 (Table 1). The deep learning tool was successful in segmenting the liver in all scans. The average standardized liver volume ± standard deviation was 1533 mL ± 375 and demonstrated a normal distribution (Fig 3). The median processing time for liver segmentation per study was 55 seconds (interquartile range, 46–81 seconds).

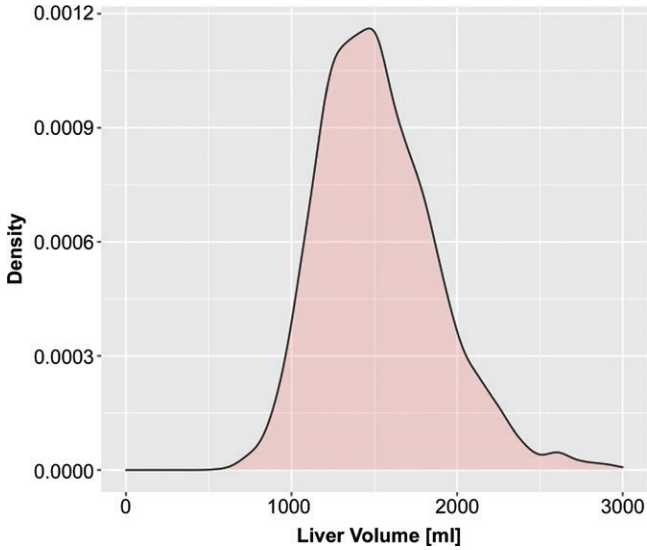

Figure 3: Density plot of automated liver volumes shows the relatively normal distribution for this generally healthy adult sample. Results for noncontrast scans have been normalized and combined with postcontrast scans. Density is a unitless measure, representing fraction of cases, where the total area under the curve sums to 1.

Linear Regression Comparisons of Patient Characteristics with Liver Volume

The initial linear regression models included BSA, but because weight was found to be a more powerful predictor of liver volume than BSA (r^2 = 0.44 and 0.36, respectively), BSA was removed from subsequent stepwise regression, as its value is directly derived from height and weight, which are already represented in the model. Table 2 shows the results of the final model in the stepwise multiple linear regression comparing patient age, sex, height, and weight with standardized liver volume. Weight, height, and age showed an independent association with liver volume (coefficients of 0.62, −0.27, and 0.05, respectively), whereas sex was not independently associated with a difference in liver volume (P = .46). Weight was the clear dominant predictor of liver volume, as seen with the scale of the standardized β coefficient in the model.

Figure 4 shows that the standardized liver volumes demonstrated a linear relationship with patient weight—which was the dominant predictive factor—with the least-squares linear regression, resulting in the following formula:

$$Liver\ volume\,(mL) = 14.0 \times (Weight[kg]) + 417.$$

The threshold for hepatomegaly was set at two standard deviations above the mean for the final modeled equation:

$$Hepatomegaly\ threshold\ volume\,(mL) = 14.0 \times (Weight[kg]) + 979.$$

This weight-dependent threshold for liver enlargement is displayed as a solid line in Figure 4.

The CC and maximal 3D linear measurements exhibited only moderate performance for identifying cases of volume-derived hepatomegaly, with many cases of under- or overestimation. A CC cutoff of 19 cm for detecting an enlarged liver (by volume definition) yielded a sensitivity of 71% (49 of 69 patients [95% CI: 60, 82]), specificity of 86% (887 of 1030 patients [95% CI: 84, 88]), positive predictive value of 26% (49 of 192 patients [95% CI: 19, 32]), and negative predictive value of 98% (887 of 907 patients [95% CI: 97, 99]). A maximal 3D line cutoff of 24 cm for detecting an enlarged liver yielded a sensitivity of 78% (54 of 69 patients [95% CI: 69, 88]), specificity of 66% (678 of 1030 patients [95% CI: 63, 69]), positive predictive value of 13% (54 of 406 patients [95% CI: 10, 17]), and negative predictive value of 98% (678 of 693 patients [95% CI: 97, 99]). Figure 1 shows an example in which a normal, more vertically oriented liver measurement was enlarged according to typical linear CC criteria but was within normal volume limits for the patient's weight. Similarly, Figure 2 depicts an enlarged liver based on our derived volume threshold, whereas the linear CC measurement did not indicate enlargement.

For the subset of 189 patients (mean age, 46 years ± 12; 77 men, 112 women) for whom we also obtained liver volume assessment with use of the semiautomated or manual software tool, the correlation between the liver volume and the deep learning tool was excellent (r^2 = 0.98; $P < .01$). The median difference in liver volume between the deep learning tool and the semiautomated or manual method was 2.3% (interquartile range, 0.7%–3.7%) (38 mL [interquartile range, 12–68 mL]). Figure 5 shows the overlap of volume distribution with each method.

Discussion

The deep learning CT tool used in this study segmented the liver for every patient evaluated, including both unenhanced and enhanced series. Our adult outpatient sample was generally healthy and asymptomatic and underwent CT imaging for either colorectal cancer screening or potential renal donation. The average liver volume ± standard deviation measured was 1533 mL ± 375, which correlated with patient weight ($P < .001$). In general, our results of liver volume assessment match well with those of smaller (n = 11–351) prior healthy study samples in investigations that used a variety of manual and semiautomated methods in terms of average values: 1493 mL (3), 1323 mL (8), 1510 mL (4), 1580 mL (7), 1419 mL (1), 1520 mL (9), 1510 mL (5), and 1671 mL (11). To establish the normal value, we decided to start with asymptomatic outpatients, but our threshold for hepatomegaly will need to be tested in symptomatic patients with known liver diseases expected to result in hepatomegaly. From the data obtained in regression analyses, we found that weight, rather than body surface area (BSA), was the major predictor of liver volume, and that sex was not an independent predictor. We also found that liver volume increased linearly with weight, which simplified the output. Furthermore, to establish the upper limit of normal, we found that elevated outliers beyond two standard deviations from the mean also increased linearly with weight. Thus, we decided that a simple linear threshold based on weight represents a good balance for characterizing true outliers (hepatomegaly). Previous research has used BSA (5), which requires additional computation and may not have the same linear relationships we found using patient weight.

Hepatomegaly is a challenging clinical and imaging diagnosis, partly because of the lack of an accepted in vivo radiologic definition. Evaluation is further complicated by acute, subacute, and chronic clinical presentations. Relevant acute causes include inflammation or hepatitis, which may be due to steatohepatitis from alcoholic-related liver disease and nonalcoholic fatty liver disease—or its more accurate name, metabolic dysfunction–associated fatty liver disease (24)—as well as viral, drug-induced, vascular, and autoimmune causes. More subacute and chronic

Table 2: Multivariable Linear Regression Analysis for Predicting Liver Volume

Variable	Standardized β Coefficient	*P* Value
Weight	0.62	<.001
Age	−0.27	<.001
Height	0.05	.002
Sex	Excluded	.46

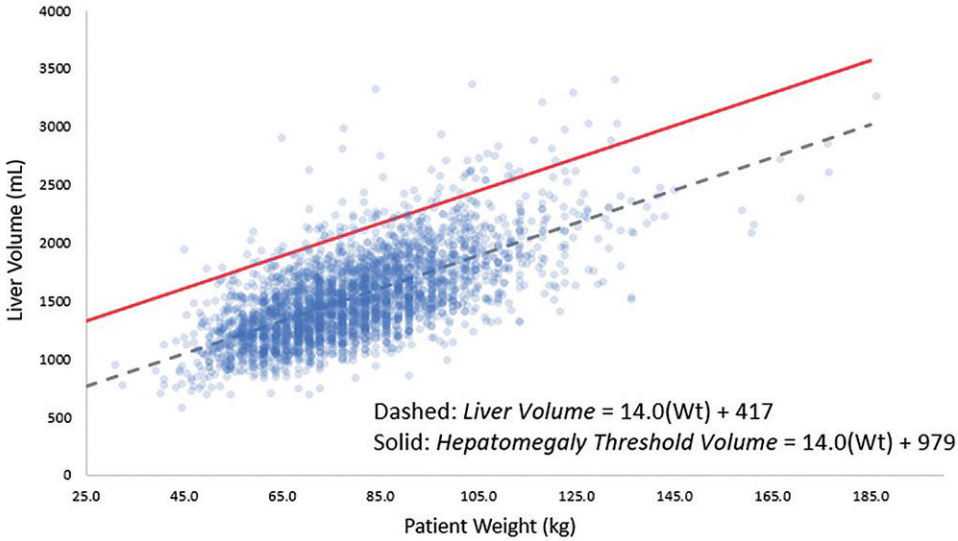

Figure 4: Graph shows automated CT-based liver volume according to patient weight (Wt). Weight was the dominant patient factor affecting liver volume. The solid red line represents the derived weight-based threshold for hepatomegaly based on two standard deviations above the mean (dashed line).

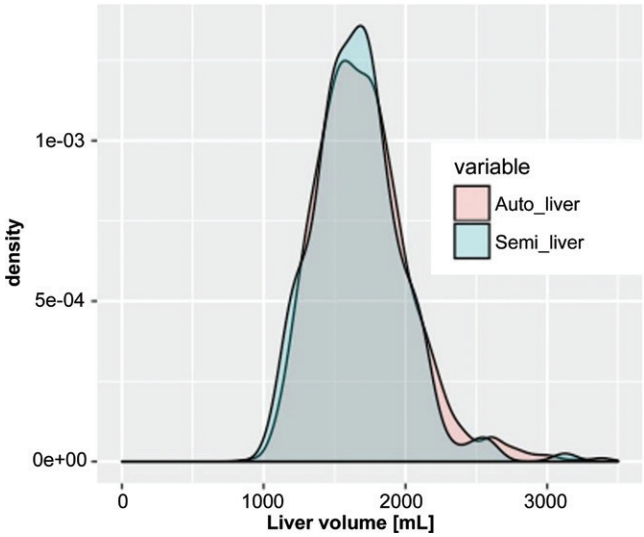

Figure 5: The density plot of the subanalysis comparing automated (Auto) liver volume (orange) and manual or semiautomated (Semi) liver volume (green) show good overlap in the distributions. The median volume difference was less than 3%.

causes include neoplastic disease (metastatic or primary tumor) as well as several metabolic, infiltrative, and congenital conditions. The correlation with liver enzymes can help distinguish hepatocellular from cholestatic causes, but these are generally nonspecific and often require additional clinical correlation and testing. Regardless of the cause, linear measurements at US, CT, or MRI provide only a crude assessment of liver size, reflected by the wide array of suggested measurements and thresholds, whereas volume estimation provides for the most logical and accurate assessment of the amount of liver tissue. Owing to technical limitations, volume assessment in cross-sectional imaging is largely limited to the research realm. However, with artificial intelligence deep learning approaches, organ volume assessment is now a feasible routine measurement that can be applied to other abdominal organs, such as the spleen.

Beyond the objective assessment of liver size by means of determination of volume, both CT and MRI can provide noninvasive assessment of liver fat content and liver fibrosis. Attenuation values obtained using unenhanced CT have a linear relationship with MRI-based proton density fat fraction (25,26), which is the current clinical standard. Automated mean whole-liver attenuation can be combined with volume assessment with use of artificial intelligence approaches (27,28). MRI elastography is a well-established tool to estimate liver fibrosis (29). However, several objective CT-based measurements can also be used to accurately predict the presence and degree of liver fibrosis, including liver surface nodularity, segmental volume changes, and parenchymal textural analysis (23,30–32). However, decreased total liver volume is actually a poor predictor of the liver fibrosis stage, primarily because of compensatory changes of Couinaud segments I–III relative to segments IV–VIII. This segmental redistribution, however, can be captured by the liver segmental volume ratio (11,23). We are currently working on a deep learning prototype for assessing segmental liver volume changes. In terms of hepatomegaly, our derived volume threshold now needs to be tested in mixed symptomatic cohorts to assess its utility.

Among the patients who underwent renal donor evaluation and had both pre- and postcontrast studies that included the entire liver, the postcontrast liver volume estimations were slightly but systematically larger than those in the precontrast equivalents, which could be described with a simple linear correlation. This minor (3.6%) discrepancy might be attributed in part to an actual physiologic increase as well as "pseudo-enlargement" related to the contrast enhancement effect that slightly expands the edges of liver segmentation. Because most abdominal CT scans are contrast enhanced, we decided to standardize all unenhanced volumes to contrast-enhanced equivalents.

We acknowledge some limitations to our study. First, based on our findings that patient weight was the major determinant, we chose to define hepatomegaly in terms of otherwise healthy outliers that were two standard deviations above the mean for a specific patient weight. This simplistic approach avoided the need for complex multivariate thresholding or nomograms, potentially allowing for easier clinical use if validated in symptomatic cohorts. Other researchers have used different approaches, including one– and 2.5–standard deviation thresholds using BSA-normalized livers (5). In future validation studies that include diseased populations, other volume thresholds may be explored. Additionally, more diverse populations from other centers and regions can be included for more generalizable results. Second, the lack of another reference standard definition of hepatomegaly beyond volume estimation may make further validation somewhat challenging. As we have demonstrated, linear measurements, such as CC assessment, cannot accurately predict liver size (ie, volume).

In summary, using a deep learning tool to measure liver volume, we derived a simple weight-based threshold for hepatomegaly that holds several advantages over the standard linear assessment used in routine clinical practice. Further validation of our simplified hepatomegaly approach is required, especially in terms of its application to more diverse symptomatic cohorts with diseased livers. Future studies on a deep learning prototype could provide additional value in assessing segmental liver volume changes. If this current approach is further validated in larger healthy and patient cohorts, then it could provide for an easier and more objective measurement of liver size with value in screening for patients with an abdominal CT scan or for diagnostic purposes.

Acknowledgment: We thank Oliver F. Hunt, MD, for his work in collecting semiautomated liver volumes for subanalysis comparison with automated volume tools.

Author contributions: Guarantor of integrity of entire study, A.A.P.; study concepts/study design or data acquisition or data analysis/interpretation, all authors; manuscript drafting or manuscript revision for important intellectual content, all authors; approval of final version of submitted manuscript, all authors; agrees to ensure any questions related to the work are appropriately resolved, all authors; literature research, A.A.P., V.N.K., M.G.L., P.M.G., P.J.P.; clinical studies, A.A.P., V.N.K., M.G.L., P.J.P.; statistical analysis, A.A.P., V.N.K., P.M.G.; and manuscript editing, A.A.P., M.G.L., P.M.G., J.W.G., D.C.E., P.J.P.

Disclosures of Conflicts of Interest: A.A.P. No relevant relationships. **V.N.K.** No relevant relationships. **M.G.L.** Prior grant funding from Philips and Ethicon; honorarium for a lecture from the International Society for Computed Tomography.

P.M.G. No relevant relationships. **J.W.G.** No relevant relationships. **D.C.E.** No relevant relationships. **R.M.S.** Cooperative Research and Development Agreement from PingAn; royalties or licenses for patents, software, or both from PingAn, iCAD, Philips, ScanMed, and Translation Holdings; graphics processing unit card donations from NVIDIA. **P.J.P.** Consulting fees from Zebra Medical Systems, GE Healthcare, and Bracco.

References

1. Andersen V, Sonne J, Sletting S, Prip A. The volume of the liver in patients correlates to body weight and alcohol consumption. Alcohol Alcohol 2000;35(5):531–532.
2. Feng LM, Wang PQ, Yu H, et al. New formula for predicting standard liver volume in Chinese adults. World J Gastroenterol 2017;23(27):4968–4977.
3. Henderson JM, Heymsfield SB, Horowitz J, Kutner MH. Measurement of liver and spleen volume by computed tomography. Assessment of reproducibility and changes found following a selective distal splenorenal shunt. Radiology 1981;141(2):525–527.
4. Kwo PY, Ramchandani VA, O'Connor S, et al. Gender differences in alcohol metabolism: relationship to liver volume and effect of adjusting for body mass. Gastroenterology 1998;115(6):1552–1557.
5. Linguraru MG, Sandberg JK, Jones EC, Petrick N, Summers RM. Assessing hepatomegaly: automated volumetric analysis of the liver. Acad Radiol 2012;19(5):588–598.
6. Poovathumkadavil A, Leung KF, Al Ghamdi HM, Othman IeH, Meshikhes AW. Standard formula for liver volume in Middle Eastern Arabic adults. Transplant Proc 2010;42(9):3600–3605.
7. Sandrasegaran K, Kwo PW, DiGirolamo D, Stockberger SM Jr, Cummings OW, Kopecky KK. Measurement of liver volume using spiral CT and the curved line and cubic spline algorithms: reproducibility and interobserver variation. Abdom Imaging 1999;24(1):61–65.
8. Stapakis J, Stamm E, Townsend R, Thickman D. Liver volume assessment by conventional vs. helical CT. Abdom Imaging 1995;20(3):209–210.
9. Suzuki K, Epstein ML, Kohlbrenner R, et al. Quantitative radiology: automated CT liver volumetry compared with interactive volumetry and manual volumetry. AJR Am J Roentgenol 2011;197(4):W706–W712.
10. Um EH, Hwang S, Song GW, et al. Calculation of standard liver volume in Korean adults with analysis of confounding variables. Korean J Hepatobiliary Pancreat Surg 2015;19(4):133–138.
11. Furusato Hunt OM, Lubner MG, Ziemlewicz TJ, Muñoz Del Rio A, Pickhardt PJ. The liver segmental volume ratio for noninvasive detection of cirrhosis: comparison with established linear and volumetric measures. J Comput Assist Tomogr 2016;40(3):478–484.
12. Heymsfield SB, Fulenwider T, Nordlinger B, Barlow R, Sones P, Kutner M. Accurate measurement of liver, kidney, and spleen volume and mass by computerized axial tomography. Ann Intern Med 1979;90(2):185–187.
13. Cai W, He B, Fan Y, Fang C, Jia F. Comparison of liver volumetry on contrast-enhanced CT images: one semiautomatic and two automatic approaches. J Appl Clin Med Phys 2016;17(6):118–127.
14. Nakayama Y, Li Q, Katsuragawa S, et al. Automated hepatic volumetry for living related liver transplantation at multisection CT. Radiology 2006;240(3):743–748.
15. Wang K, Mamidipalli A, Retson T, et al. Automated CT and MRI liver segmentation and biometry using a generalized convolutional neural network. Radiol Artif Intell 2019;1(2):180022.
16. Mosteller RD. Simplified calculation of body-surface area. N Engl J Med 1987;317(17):1098.
17. Pickhardt PJ, Graffy PM, Zea R, et al. Automated abdominal CT imaging biomarkers for opportunistic prediction of future major osteoporotic fractures in asymptomatic adults. Radiology 2020;297(1):64–72.
18. Perez AA, Pickhardt PJ, Elton DC, Sandfort V, Summers RM. Fully automated CT imaging biomarkers of bone, muscle, and fat: correcting for the effect of intravenous contrast. Abdom Radiol (NY) 2021;46(3):1229–1235.
19. Çiçek Ö, Abdulkadir A, Lienkamp SS, Brox T, Ronneberger O. Medical Image Computing and Computer-Assisted Intervention 3D U-Net: Learning Dense Volumetric Segmentation from Sparse Annotation. MICCAI 2016. Cham, Switzerland: Springer, 2016; 424–432.
20. Kayalibay B, Jensen G, van der Smagt P. CNN-based segmentation of medical imaging data. arXiv preprint arXiv:1701.03056. https://arxiv.org/abs/1701.03056. Posted January 11, 2017. Accessed February 25, 2021.
21. Sandfort V, Yan K, Pickhardt PJ, Summers RM. Data augmentation using generative adversarial networks (CycleGAN) to improve generalizability in CT segmentation tasks. Sci Rep 2019;9(1):16884.
22. Medical Segmentation Decathlon. Generalisable 3D Semantic Segmentation. https://arxiv.org/abs/2106.05735. Accessed February 25, 2021.
23. Pickhardt PJ, Malecki K, Hunt OF, et al. Hepatosplenic volumetric assessment at MDCT for staging liver fibrosis. Eur Radiol 2017;27(7):3060–3068.
24. Fouad Y, Waked I, Bollipo S, Gomaa A, Ajlouni Y, Attia D. What's in a name? Renaming 'NAFLD' to 'MAFLD'. Liver Int 2020;40(6):1254–1261.
25. Guo Z, Blake GM, Li K, et al. Liver fat content measurement with quantitative CT validated against MRI proton density fat fraction: a prospective study of 400 healthy volunteers. Radiology 2020;294(1):89–97.
26. Pickhardt PJ, Graffy PM, Reeder SB, Hernando D, Li K. Quantification of liver fat content with unenhanced MDCT: phantom and clinical correlation with MRI proton density fat fraction. AJR Am J Roentgenol 2018;211(3):W151–W157.
27. Graffy PM, Sandfort V, Summers RM, Pickhardt PJ. Automated liver fat quantification at nonenhanced abdominal CT for population-based steatosis assessment. Radiology 2019;293(2):334–342.
28. Pickhardt PJ, Blake GM, Graffy PM, et al. Liver steatosis categorization on contrast-enhanced CT using a fully automated deep learning volumetric segmentation tool: evaluation in 1204 healthy adults using unenhanced CT as a reference standard. AJR Am J Roentgenol 2021;217(2):359–367.
29. Tang A, Cloutier G, Szeverenyi NM, Sirlin CB. Ultrasound elastography and MR elastography for assessing liver fibrosis: part 2, diagnostic performance, confounders, and future directions. AJR Am J Roentgenol 2015;205(1):33–40.
30. Lubner MG, Jones D, Kloke J, Said A, Pickhardt PJ. CT texture analysis of the liver for assessing hepatic fibrosis in patients with hepatitis C virus. Br J Radiol 2019;92(1093):20180153.
31. Pickhardt PJ, Graffy PM, Said A, et al. Multiparametric CT for noninvasive staging of hepatitis C virus–related liver fibrosis: correlation with the histopathologic fibrosis score. AJR Am J Roentgenol 2019;212(3):547–553.
32. Roberts AS, Shetty AS, Mellnick VM, Pickhardt PJ, Bhalla S, Menias CO. Extramedullary haematopoiesis: radiological imaging features. Clin Radiol 2016;71(9):807–814.